UNIVERSITY OF CAMBRIDGE
Faculty of Economics

Institute for
New Economic Thinking

CAMBRIDGE WORKING PAPERS IN ECONOMICS
CAMBRIDGE-INET WORKING PAPERS

On Time Trend of COVID-19: A Panel Data Study

Chaohua Dong	Jiti Gao	Oliver Linton	Bin Peng
Zhongnan University of Economics and Law	Monash University	University of Cambridge	Monash University

Abstract

In this paper, we study the trending behaviour of COVID-19 data at country level, and draw attention to some existing econometric tools which are potentially helpful to understand the trend better in future studies. In our empirical study, we find that European countries overall flatten the curves more effectively compared to the other regions, while Asia & Oceania also achieve some success, but the situations are not as optimistic as in Europe. Africa and America are still facing serious challenges in terms of managing the spread of the virus and reducing the death rate. In Africa, the rate of the spread of the virus is slower and the death rate is also lower than those of the other regions. By comparing the performances of different countries, our results on the performance of different countries in managing the speed of the virus agree with Gu et al. (2020). For example, both studies agree that countries such as USA, UK and Italy perform relatively poorly; on the other hand, Australia, China, Japan, Korea, and Singapore perform relatively better.

Reference Details

On Time Trend of COVID-19: A Panel Data Study[1]

Chaohua Dong[†] and Jiti Gao[‡] and Oliver Linton[⋆] and Bin Peng[‡]

[†]Zhongnan University of Economics and Law
[‡]Monash University
[⋆]University of Cambridge

June 23, 2020

Abstract

In this paper, we study the trending behaviour of COVID-19 data at country level, and draw attention to some existing econometric tools which are potentially helpful to understand the trend better in future studies. In our empirical study, we find that European countries overall flatten the curves more effectively compared to the other regions, while Asia & Oceania also achieve some success, but the situations are not as optimistic as in Europe. Africa and America are still facing serious challenges in terms of managing the spread of the virus and reducing the death rate. In Africa, the rate of the spread of the virus is slower and the death rate is also lower than those of the other regions. By comparing the performances of different countries, our results on the performance of different countries in managing the speed of the virus agree with Gu et al. (2020). For example, both studies agree that countries such as USA, UK and Italy perform relatively poorly; on the other hand, Australia, China, Japan, Korea, and Singapore perform relatively better.

Keywords: COVID-19, Deterministic time trend, Panel data, Varying-coefficient

JEL classification: C23, C54

1   Introduction

Words like "exponential rate" and "flatten the curve" have been widely cited by all sorts of social media since the outbreak of the pandemic coursed by COVID-19. Since early 2020, governments of the entire world have been frequently updating their policies in order to manage the spread of the virus, and reduce the death rate while constrained by limited medical resources. Understanding the trending behaviour of the pandemic is therefore crucial from the perspective of policy making.

The paper investigates the trending behaviour of COVID-19 data at country level, and draws attention to some existing econometric tools which are potentially helpful in future work. Trend modelling of COVID-19 data is challenging due to the following reasons at least. First, each country shows a dominating deterministic trend, which wipes out other information. Second, the policy of each country has been updated frequently during the pandemic, so analysis using constant parameters may not reflect these impacts properly. Third, time series analysis cannot be conducted for some countries due to small sample, while pooling data together yields a highly unbalanced dataset. In this study, we aim to model the aforementioned challenges, raise some difficulties, and call for studies which can account for these features simultaneously.

Based on our investigation, we find the following econometric literature is particularly useful. Deterministic time trend modelling (such as Phillips, 2007, Robinson, 2012 and Gao et al., 2020) helps address the first challenge. Time-varying coefficient models which date back to Robinson (1989, 1991) or works even earlier are useful to address the second challenge. In some recent studies, both Gu et al. (2020) and Linton (2020) conduct time series analysis on COVID-19 data of selected countries for different purposes, while Liu et al. (2020) forecast infection of COVID-19 using panel data by a Bayesian methodology. They all agree that time-varying coefficients should be adopted to investigate pandemic data. Factor models and relevant data imputation techniques are closely related to the first and third challenges (e.g., Bai and Ng, 2002, 2019, Su and Wang, 2017, and Su et al., 2019). It is noteworthy that Bai and Ng (2019) and Su et al. (2019) have worked out that certain types of random missing data can be dealt within the framework of factor analysis effectively.

In our empirical study, we find that European countries overall flatten the curves more effectively compared to the other regions, while Asia & Oceania also achieve some success, but the situations are not as optimistic elsewhere. Africa and America are still facing serious challenges in terms of managing the spread of the virus, and reducing the death rate, although in Africa the virus spreads slower and has a lower death rate than the other regions. By comparing the performances of different countries, our results incidentally agree with Gu et al. (2020), though different approaches and models are considered. For example, both works agree that countries

such as USA, UK and Italy perform relatively poorly; on the other hand, Australia, China, Japan, Korea, and Singapore perform relatively better.

The rest of this paper is as follows. Section 2 presents the model, and the estimation strategy with associated asymptotic properties. In section 3, we provide our empirical findings. Section 4 concludes. Theoretical development, tables and figures are provided in the appendix.

Before proceeding further, it is convenient to introduce some notation that will be used throughout this paper. $\lfloor A \rfloor$ means the largest integer not exceeding A; $K(\cdot)$ and h represent a kernel function and a bandwidth of the nonparametric kernel method, respectively; $K_h(u) = K(u/h)/h$; $\mathbb{I}(\cdot)$ stands for the indicator function; $\text{diag}\{A_1, \ldots, A_k\}$ means constructing a diagonal matrix from $A_1, \ldots, A_k$.

2 Methodology

In this section, we consider two models which we believe are useful to investigate the time trend of COVID-19.

2.1 Model 1

We now present the first model, which captures the trend aspect. The countries, indexed by $i = 1, \ldots, N$, start experiencing the virus at different time points $b_{iT} \in \{1, \ldots, T\}$. For many countries we may have $b_{iT} = 1$, but not all of them. We now propose the following model:

$$y_{it} = \begin{cases} g_i(\tau_t)|t - \beta_{t,b_{iT}}|^a + \varepsilon_{it}, & \text{for } t \geq b_{iT} \\ 0, & \text{otherwise} \end{cases} \tag{2.1}$$

In model (2.1), y_{it} is the logarithm of the observed number of new cases (plus one to include days that have zero outcomes and is thus zero when there is no either observed case or infection/death). ε_{it} is an error term capturing information less dominating than the trend. Further assumptions will be imposed on ε_{it} later to account for potential omitting variable issues, to capture second tier information over time, and to allow for certain types of heterogeneity. Theoretically, $\beta_{t,b_{iT}}$ may be unknown. Practically, $\beta_{t,b_{iT}}$ accounts for the impacts of different starting points, and may have different forms depending on the research questions. A commonly used form of $\beta_{t,b_{iT}}$ may be $\beta_{t,b_{iT}} \equiv b_{iT} - 1$. This is not the main focus of the paper, as it does not impact on our empirical study very much. The trend of (2.1) can be regarded as a common feature of the virus. Specifically, the value of a characterizes the rate of infection or death. Larger a indicates a faster rate. $g_i(\cdot)$ is a function to reflect the change of policy over time for the country i, and captures some heterogeneous features across countries.

We can regard (2.1) as a panel data version of Gao et al. (2020) with an extra moving mean $\beta_{t,b_{iT}}$. This raises a few challenges that are raised in both the main text and the online supplementary appendix. Before proceeding further, we impose a condition to quantify the impacts of missing values. Specifically, suppose that there exist a sequence of fixed points $\{b_1^*, \ldots, b_N^*\}$ and a known function $\beta^*(\cdot, \cdot)$ such that

$$
\begin{aligned}
&(1). \quad \max_{i \geq 1} \left| \frac{b_{iT}}{T} - b_i^* \right| = O(T^{-\nu_1}), \\
&(2). \quad \max_{i \geq 1} \left| \left\| \frac{t - \beta_{t,b_{iT}}}{T} \right\|^a - \beta^*(\tau_t, b_i^*) \right| \leq C_0\, T^{-\nu_2},
\end{aligned} \tag{2.2}
$$

where $0 \leq C_0 < \infty$, ν_1 and ν_2 are fixed constants satisfying that $0 < \nu_1 \leq 1$ and $\nu_2 > 0$. When $\beta_{t,b_{iT}} \equiv b_{iT} - 1$ and $\beta^*(\tau_t, b_i^*) = |\tau_t - b_i^*|^a$, part (2) of (2.2) holds trivially. Without missing values, b_{iT}'s and b_i^*'s reduce to 1 and 0 respectively. Practically, the values of b_{iT}'s and b_i^*'s can be controlled by removing a reasonable range of periods from the beginning in order to reduce the impacts of missing values. In practice, one has to find a balance between available sample size and the impact of missing data.

We are interested in recovering information under the framework of (2.1)-(2.2). To carry on our analysis, we write (2.1) in vector form.

$$
Y_t = \mathbb{I}_t G(\tau_t) + \mathbb{I}_t \mathcal{E}_t, \tag{2.3}
$$

where $\mathbb{I}_t = \mathrm{diag}\{\mathbb{I}(t \geq b_{1T}), \ldots, \mathbb{I}(t \geq b_{NT})\}$, $Y_t = (y_{1t}, \ldots, y_{Nt})'$, $\mathcal{E}_t = (\varepsilon_{1t}, \ldots, \varepsilon_{Nt})'$, and

$$
G(\tau_t) = (g_1(\tau_t)|t - \beta_{t,b_{1T}}|^a, \ldots, g_N(\tau_t)|t - \beta_{t,b_{NT}}|^a)'.
$$

Since $G(\cdot)$ is unknown, we adopt the nonparametric kernel approach, and multiply $K_h^{1/2}(\tau_t - u)$ for both sides of (2.3). Given τ_t in a small neighbour of u, we obtain

$$
\frac{G(\tau_t)}{T^a} K_h^{1/2}(\tau_t - u) \approx \mathcal{G}(u), \tag{2.4}
$$

where $\mathcal{G}(u) = (g_1(u)\beta^*(u, b_1^*), \ldots, g_N(u)\beta^*(u, b_N^*))'$. Thus, after proper normalization (i.e., T^a), (2.4) is the leading vector when analysing $Y_t K_h^{1/2}(\tau_t - u)$. However, a is unknown, so has to be estimated.

In view of (2.3)-(2.4) and motivated by the construction of the Financial Stress Index[2], we conduct the principle component analysis on the sample quantity

---

[2] The largest eigenvalue and the associated eigenvector is calculated using 18 weekly data series in order to measure the degree of financial stress in the markets. See St. Louis Fed's website for details. https://fred.stlouisfed.org/series/STLFSI2

$$\Sigma(u) = \frac{1}{NT} \sum_{t=1}^{T} Y_t Y_t' K_h(\tau_t - u) \tag{2.5}$$

for all u.

We briefly explain the intuition below. Note that simple algebra yields

$$\Sigma(u) = \frac{1}{NT} \sum_{t=1}^{T} \mathbb{I}_t G(\tau_t) G(\tau_t)' \mathbb{I}_t K_h(\tau_t - u)$$

$$+ \frac{1}{NT} \sum_{t=1}^{T} \mathbb{I}_t \mathcal{E}_t \mathcal{E}_t' \mathbb{I}_t K_h(\tau_t - u) + \text{interaction terms}. \tag{2.6}$$

Loosely speaking, $\frac{1}{NT} \sum_{t=1}^{T} \mathbb{I}_t G(\tau_t) G(\tau_t)' \mathbb{I}_t K_h(\tau_t - u)$ of (2.6) contains a quadratic in the time trend that will dominates the other terms. As a consequence, the largest eigenvalue and the associated eigenvector of $\Sigma(u)$ reflect the information associated with $\frac{1}{NT} \sum_{t=1}^{T} \mathbb{I}_t G(\tau_t) G(\tau_t)' \mathbb{I}_t K_h(\tau_t - u)$ only, which allows us to focus on the trending properties of the virus, and ignore the secondary information asymptotically. To explain the intuition using an even simpler example, one may consider conducting an OLS regression for $y_t = \rho t + \varepsilon_t$, where as long as ε_t is not diverging faster than t, the information of ρ can always be retrieved.

That said, let λ_u and ℓ_u be the largest eigenvalue and the corresponding eigenvector of $\Sigma(u)$, and $\|\ell_u\| = 1$. Mathematically, it is written as

$$\lambda_u \ell_u = \Sigma(u) \ell_u. \tag{2.7}$$

Accounting for the unbalancedness of the data, we further define the following set:

$$\mathbb{C} = \left\{ t \mid t = 1, \ldots, T, \ \lim_{N \to \infty} \frac{\sharp \mathbb{N}_{\tau_t}}{N} = 1 \right\},$$

where $\mathbb{N}_u = \{ i \mid b_i^* \leq u - h, 1 \leq i \leq N \}$, and $\sharp \mathbb{N}_u$ represents the cardinality of $\mathbb{N}_u$. Let $\mathbb{N}_u^c = \{ 1, \ldots, N \} \setminus \mathbb{N}_u$. By construction, $\mathbb{C}$ rules out a set of time periods that we cannot make inference on due to the availability of data. In practice, we may let $\sharp \mathbb{N}_{\tau_t} \geq N - \ln N$, which replaces the limit in the definition of $\mathbb{C}$ as a practical guide to choose $\mathbb{C}$. Alternatively, we can let $\mathbb{C} = \{ \max_{i \geq 1} b_{iT} - c, \ldots, T \}$ with c being a reasonably small positive integer for feasibility and simplicity.

Finally, the estimator of a is presented as follows.

$$\widehat{a} = \frac{1}{2 \ln T} \cdot \ln \left\{ \frac{1}{\sharp \mathbb{C}} \sum_{t \in \mathbb{C}} \lambda_{\tau_t} \right\}. \tag{2.8}$$

Intuitively, $\frac{1}{\sharp \mathbb{C}} \sum_{t \in \mathbb{C}} \lambda_{\tau_t}$ yields an estimate of $O(T^{2a})$ using (2.6), so the logarithm of $\frac{1}{\sharp \mathbb{C}} \sum_{t \in \mathbb{C}} \lambda_{\tau_t}$ is divided by $2 \ln T$ to yield an estimate of a.

4

Below, we present our assumptions and give some justifications.

Assumption 1

1. Let $K(\cdot)$ be a function defined on $[-1, 1]$, $K^{(1)}(w)$ be uniformly bounded on $[-1, 1]$, $\int_{-1}^{1} K(w)dw = 1$ and $\int_{-1}^{1} |w|K(w)dw < \infty$. Suppose that $h \to 0$ and $Th \to \infty$.

2. (a) Suppose that $\max_{i \geq 1} \sup_{\tau \in \mathbb{D}} |F_i(\tau)| < \infty$, where $F_i(\tau) = g_i(\tau)\beta^*(\tau, b_i^*)$ and $\mathbb{D} = [\inf_{t \in \mathbb{C}} \tau_t, 1]$. As $w \to 0$, let $\max_{i \geq 1} \sup_{\tau \in \mathbb{D}} |F_i(\tau + w) - F_i(\tau)| \leq c|w|^{\mu}$, where μ and $c > 0$ are fixed constants.

   (b) There exists a function $\bar{g}(u)$ such that $\sup_{u \in \mathbb{D}} |\frac{1}{N}\mathcal{G}(u)'\mathcal{G}(u) - \bar{g}(u)^2| = O(\phi_{2,N})$, where $\phi_{2,N} \to 0$, $\int_{\mathbb{D}} \bar{g}(u)^2 du = 1$, and $\mathcal{G}(\cdot)$ is defined in (2.4).

3. Suppose that $\sup_{u \in \mathbb{D}} \frac{1}{NT} \sum_{t=1}^{T} \mathcal{E}_t' \mathcal{E}_t K_h(\tau_t - u) = O_P(\delta_T)$, and $\delta_T/T^{2a} \to 0$.

Assumption Assumption 1.1 imposes restrictions on the kernel function and the bandwidth, which are standard in the literature of kernel regression (Li and Racine, 2006).

In Assumption 1.2.a, the condition on $F_i(\tau)$ requires Lipschitz continuity. It can be further decomposed by putting restrictions on a, $\beta^*(\cdot, \cdot)$ and $g_i(\cdot)$'s, but it will lead to quite lengthy notation and development. Assumption 1.2.b imposes an identification restriction. The condition $\int_{\mathbb{D}} \bar{g}(u)^2 du = 1$ fixes the location of $\bar{g}(u)$ along Y-axis, and it has no impact on the quantities in relative terms that we shall explore in the empirical study.

As the error terms include information less dominating than the trend, all we require in Assumption 1.3 is that the magnitude of the secondary information does not overwhelm the trend presented by the virus, which can be regarded as how we model the omitting variable issues in the current setting.

We are now ready to present the asymptotic results associated with our empirical investigation.

Theorem 2.1. *Consider the model stated in (2.1) and (2.2). Under Assumption 1, as $(N, T) \to (\infty, \infty)$,*

1. *$\sup_{u \in \mathbb{D}} \|\ell_u \ell_u' - P_{\mathcal{G}(u)}\| = O_P(\phi_{1,NT})$, and $\sup_{u \in \mathbb{D}} \left|\frac{\lambda_u}{T^{2a}} - \frac{\mathcal{G}(u)'\mathcal{G}(u)}{N}\right| = O_P(\phi_{1,NT})$;*

2. *$\widehat{a} - a = O_P(\frac{\phi_{1,NT} + \phi_{2,N}}{\ln T})$,*

where $\phi_{1,NT} = \frac{\delta_T^{1/2}}{T^a} + \left\{\frac{1}{T^{\min\{\nu_1, \nu_2\}}} + \frac{\sharp \mathbb{N}_u^c}{N} + h^{\mu}\right\}^{1/2}$, and $P_{\mathcal{G}(u)} = \mathcal{G}(u)\{\mathcal{G}(u)'\mathcal{G}(u)\}^{-1}\mathcal{G}(u)'$. In addition, suppose $b_i^* = 0$ for $i \geq 1$.

3. *For $\forall t, s \in \mathbb{C}$, $R_{ts} - \frac{\beta^*(\tau_t, 0)^2}{\beta^*(\tau_s, 0)^2} \cdot \frac{\|\mathbb{G}(\tau_t)\|^2}{\|\mathbb{G}(\tau_s)\|^2} = O_P(\phi_{1,NT})$;*

5

4. For $\forall i, j \in \mathbb{N}_u$, $\sup_{u \in \mathbb{D}} \left| Q_{u,ij} - \frac{g_i(u)}{g_j(u)} \right| = O_P(\phi_{1,NT})$,

where $R_{ts} = \frac{\lambda_{\tau_t}}{\lambda_{\tau_s}}$, $\mathbb{G}(u) = (g_1(u), \ldots, g_N(u))'$, $Q_{u,ij} = \frac{\ell_{u,i}}{\ell_{u,j}}$, and $\ell_{u,i}$ stands for the ith element of ℓ_u.

With a balanced dataset, the terms involving ν_1, ν_2, μ and $\sharp\mathbb{N}_u^c$ in the above theorem will vanish, and the asymptotic development will be much simplified. Utilizing panel data, the rate of the second result improves the slow rate of Theorem 4.2 of Gao et al. (2020), wherein a detailed explanation can be found.

The first result explains how the unbalancedness of the data affects the asymptotic results. Also, it implies that we can recover the space spanned by $\mathcal{G}(u)$. Under the conditions $b_i^* = 0$ for $i \geq 1$, the result will reduce to $\sup_{u \in \mathbb{D}} \|\ell_u \ell_u' - P_{\mathbb{G}(u)}\| = O_P(\phi_{1,NT})$. It is noteworthy that the condition $b_i^* = 0$ for $i \geq 1$ indicates that the missing value is negligible in the asymptotic analysis, which can be controlled by choosing $\mathbb{C}$ in practice.

For the third result, without loss of generality, suppose that $t > s$. Note that there are two ratios involved in R_{ts}, i.e., $\frac{|\beta^*(\tau_t,0)|}{|\beta^*(\tau_s,0)|}$ and $\frac{\|\mathbb{G}(\tau_t)\|}{\|\mathbb{G}(\tau_s)\|}$. It is not hard to see that the ratio $\frac{|\beta^*(\tau_t,0)|}{|\beta^*(\tau_s,0)|}$ measures the rate associated with the virus, while the ratio $\frac{\|\mathbb{G}(\tau_t)\|}{\|\mathbb{G}(\tau_s)\|}$ reflects the efforts that the countries make to flatten the curves. For effective policies, the ratio R_{ts} should be lower than 1.

The fourth result is also about a ratio that provides a way of comparing the effectiveness of two different policies at the same time point. Note that $g_i(\cdot)$'s model the effectiveness of the policies. A lower value of $g_i(\cdot)$ indicates better efforts in terms of flattening the curve. Thus, if $0 < \frac{g_i(u)}{g_j(u)} < 1$, we may conclude the country i has a more effective policy compared to the country j. Otherwise, the country j performs relatively better.

Finally, we comment on how $g_i(\cdot)$'s and $\beta^*(\cdot, \cdot)$ can be recovered. Since $\beta^*(\cdot, \cdot)$ and $g_i(\cdot)$'s exist in the model through a multiplication form, they cannot be individually estimated without further identification restrictions. If one is willing to impose a restriction (such as $\frac{\mathbb{G}(u)'\mathbb{G}(u)}{N} = 1$), then $\beta^*(\cdot, \cdot)$ can be recovered as suggested by the second argument of Theorem 2.1.1. If the form of $\beta^*(\cdot, \cdot)$ was known, the asymptotic distribution associated with the estimate of each $g_i(\cdot)$ can be constructed as in Theorem 4.3 of Gao et al. (2020). Alternatively, Theorem 2.1.4 suggests that for any given u we may pick an individual i as a benchmark, then recover the rest $g_j(u)$'s and $\beta^*(\cdot, \cdot)$ utilizing the ratio of the fourth result. As these are not the main focus of this paper, we leave the choice of identification strategy to future study. In our empirical work we will emphasise the identified quantities: a, and the ratios $R*_{ts} = \frac{\beta^*(\tau_t,0)^2}{\beta^*(\tau_s,0)^2} \cdot \frac{\|\mathbb{G}(\tau_t)\|^2}{\|\mathbb{G}(\tau_s)\|^2}$ and $Q(u) = \frac{g_i(u)}{g_j(u)}$.

2.2 Model 2

We consider a second model that is designed to capture a single peaked epidemic trajectory, similar to Linton (2020). We consider the following regression

$$y_{it} = \begin{cases} \gamma_i - g_i(\tau_t)|t - \beta_{t,b_{iT}}|^a + \varepsilon_{it}, & \text{for } t \geq b_{iT} \\ 0, & \text{otherwise} \end{cases}, \tag{2.9}$$

where γ_i is the global maximum of each individual. When $t = \beta_{t,b_{iT}}$, the global maximum is achieved at γ_i.

If we have a complete trajectory of the epidemic, or at least data that includes the peak and sometime afterwards, we may estimate γ_i directly. Specifically, we may take any local (in time) smoother and maximize this over time. The smoothing method eliminates the error term and then the resulting function is uniquely maximized at the true peak time. One then can use the methodology of Section 2.1 to work with the transformed model as follows.

$$y_{it}^* = \begin{cases} g_i(\tau_t)|t - \beta_{t,b_{iT}}|^a + \varepsilon_{it}^*, & \text{for } t \geq b_{iT} \\ 0, & \text{otherwise} \end{cases}, \tag{2.10}$$

where $y_{it}^* = \widehat{\gamma}_i - y_{it}$ and $\varepsilon_{it}^* = -\varepsilon_{it} + (\widehat{\gamma}_i - \gamma_i)$.

Additionally, one may consider an estimation strategy that tries to estimated the parameters of interest simultaneously to avoid the bias caused by the plug-in procedure. We wish to leave it to the future study, but we examine the model (2.10) using the approach of Section 2.1 in the empirical study as a robustness check.

3　Empirical Study

In this section, we investigate the time trend of the COVID-19 data. Before proceeding further, we comment on two practical issues — the choice of kernel function and the bandwidth selection procedure.

For the kernel function, we follow Hong and Li (2005) and Su and Wang (2017) to adopt a boundary adjusted kernel:

$$K((\tau_t - u)/h) = \begin{cases} \mathcal{K}((\tau_t - u)/h), & u \in [h, 1-h] \\ \mathcal{K}((\tau_t - u)/h)/\int_{-1}^{(1-u)/h} \mathcal{K}(w)dw, & u \in (1-h, 1] \end{cases}$$

for $t = 1, \ldots, T$, where $\mathcal{K}(w)$ is the Epanechnikov kernel. By construction of $\mathbb{C}$, there is no need to adjust the left boundary.

Next, we provide a bandwidth selection procedure which minimizes a leave-one-out cross validation function as follows.

$$\widehat{h} = \text{argmin}_h \text{CV}(h),$$

and

$$\mathrm{CV}(h) = \sum_{t \in \mathbb{C}} \|Y_t/(\sqrt{N}T^{a_h}) - \widehat{\ell}_{-\tau_t}\|^2,$$

where a_h is obtained from (2.8) given h, and $\widehat{\ell}_{-\tau_t}$ is obtained from (2.7) by replacing $\Sigma(\tau_t)$ with $\frac{1}{NT}\sum_{s=1,s\neq t}^{T} Y_s Y_s' K_h(\tau_s - \tau_t)$. The terms $\sqrt{N}$ and T^{a_h} are normalizers to ensure that $\widehat{\ell}_{-\tau_t}$ and the normalized Y_t are on the same scale. To examine the sensitivity of the bandwidth selection procedure, we further consider $h_L = 0.8\widehat{h}$ and $h_R = 1.2\widehat{h}$.

3.1 Data

We focus on daily new infection and new deaths from four regions[3], (i.e., Africa (AF), America (AM), Asia & Oceania (AO), and Europe (EU)); we account for population density of each country in the following analysis. Note that there are only 8 countries from Oceania in the data source, so we merge Asia and Oceania together. Population density is based on the data of 2018 from World Bank, and is measured as people per sq. km of land area. We exclude countries that do not have the population density figures. For each region, the sample period starts from the date when the first confirmed case is recorded, but we remove the first 30 days of each region in order to reduce the impacts of missing data. Finally, we summarize the available sample in Table A.1.

For infection data, the four regions have roughly the same number of countries. However, death data are very unbalanced. We remove the countries with total deaths less than 20 at 31/05/2020, which is why the number of countries drops for death data. It is not surprising that Asia & Oceania has the longest period due to early outbreak of China, while Africa has the shortest period.

3.2 Results Associated with Model (2.1)

We now start conducting numerical analysis using the approach of Section 2.1. Specifically, we consider two sets of $\{y_{it}\}$ for both infection and death.

Case 1: $\ln(\text{daily increase} + 1)$

Case 2: $\ln\left(\frac{\text{daily increase} + 1}{\text{population density}}\right)$

---

[3]The data are downloaded from European Centre for Disease Prevention and Control: https://www.ecdc.europa.eu/en/publications-data/download-todays-data-geographic-distribution-covid-19-cases-worldwide.

3.2.1 Overall Analysis

We let $\mathbb{C} = \{\lfloor T/4 \rfloor + 1, \ldots, T\}$ for simplicity, and summarize the estimates of a in Table A.2, which shows that the estimates are not overly sensitive to different choices of the bandwidth.

For infection data, Europe has the highest values of $\widehat{a}$ for both Cases 1 and 2, which could be due to overall high quality infrastructure leading to high mobility of the entire population. Moreover, America and Asia & Oceania have roughly similar values in both Cases 1 and 2, while Africa has the lowest value, which implies that the virus spreads in Africa slower than the other regions.

For death data, America has the highest death rate for both Cases 1 and 2. Although the estimates from the original data (i.e., Case 1) indicate that Africa has a very low death rate, the estimates from the normalized version (i.e., Case 2) indicates that the situation is not too optimistic but is still the best among four regions.

Next, we examine the ratio $R_{t+1,t}$ for $t = \lfloor T/4 \rfloor + 1, \ldots, T-1$ by the third result of Theorem 2.1, and plot them in Figures A.1 and A.2 for infection and death data respectively. We explore infection in Figure A.1 first. For Case 1, the curves of Africa and America are always above 1, although approaching to 1 slowly. However, for Case 2, the plot of America diverges from 1 during the entire period. Europe is the only region achieving a rate lower than 1 during April and most time of May based on the original data and normalized data. In this sense, we believe the policies of European countries are most effective. The curves of Asian & Oceania move around 1 all the time for both cases, but is slightly higher than 1 in most of the days. It is noteworthy that most curves of Figure A.1 diverging from 1 from late May, which might be due to the fact that many governments start lifting the lock-down in May. For the ratios associated with death data in Figure A.2, the patterns are almost identical to those presented in Figure A.1, so we do not repeat the discussions.

3.2.2 Comparison across Countries

In this subsection, we compare the performances of countries in each region using the fourth result of Theorem 2.1. Specifically, for each region, we let the country that has the largest value of daily increase at 31/05/2020 be the benchmark, and label it by the index $i = 1$. We summarize the reference countries in Table A.3. We then plot $Q_{\tau_t,i1}$ for $i \geq 2$ associated with infection and death in Figures A.3 and A.4 respectively, where the countries are labelled by ISO 3166-1 alpha-3 codes. In each sub-plot, the legend is ranked by $Q_{\tau_t,i1}$ from largest to smallest at the time period T. The lines in each sub-plot reflect how the corresponding countries perform at different time points compared to the reference country. As explained under Theorem 2.1, (1). smaller value indicates better performance, and (2). a value less (greater) than 1 indicates

better (worse) performance than the reference country.

Our results somewhat agree with the findings of Gu et al. (2020). For example, (1). countries such as USA, UK and Italy are at the top of the corresponding sub-plots in our investigation, which indicates ineffective performance in terms of managing the spread of the virus and reducing the death rate; (2). on the other hand, our finding also suggests that countries such as Australia, China, Japan, Korea, and Singapore perform relatively well as in Gu et al. (2020).

3.2.3 Rolling-Window Analysis

Finally, we estimate a and the ratio R using a rolling-window sample in order to capture some dynamics, which in a sense can be regarded as a robustness check on the sensitivity of the data. We prepare the data as in Section 3.1, and remove the first 40 days for each region to avoid the impacts of missing value on the 30 days rolling-window (i.e., $T = 30$ for each regression). For each window, we let $\mathbb{C} = \{26, 27, \ldots, 30\}$ and estimate $\bar{R} = \frac{1}{4} \sum_{t=26}^{29} R_{t+1,t}$. We then record the estimated a and $\bar{R}$ from the first available window till the end.

For effective policies, we expect the estimates of a show a turning point at certain stage, and expect the value of $\bar{R}$ below one. We plot the estimates of each region in Figures A.5-A.8, where the X-axis is indexed by the last day of the consecutive 30 days period.

First, we take a look at the values associated with infection in Figures A.5 and A.7. In Figure A.5, the curves of Africa and America keep increasing with a very steady rate, which is a concern from the perspective of flattening the curve. The curves of Asia & Oceania become flat gradually, but the turning points have not shown up yet. Europe is the only continent which has a turning point in Figure A.5, and the pattern exists in both Cases 1 and 2. It further supports that European countries have more effective polices overall. In Figure A.7, the curves of Asia & Oceania and Europe are approaching to 1, while the curves of Africa and America do not. Especially, the values of $\bar{R}$ of Africa start diverging from 1 from late May, which is also worrisome.

Second, we turn to the results associated with death in Figures A.6 and A.8. Clearly, in Figure A.6, the death rate of Europe has been dropping, while Asia & Oceania have managed to flatten the curve, but the turning point has not shown up yet. Africa and America have increasing death rates during the entire period. In Figure A.8, Europe still performs much better than the other regions, as it is the only region having $\bar{R}$ less than 1. The curves of Asia & Oceania have been approaching to 1, while Africa and America do not show much improvement during the period.

3.3 Results Associated with Model (2.9)

The data and the corresponding settings of this subsection are identical to those in Section 3.2, but we work with the transferred version using (2.10). Still, we consider Cases 1 and 2 for the transferred data. It is noteworthy that under the model (2.9), the interpretation on the values of a, $R_{t+1,t}$ and $Q_{\tau_t,i1}$ are respectively different from those in Section 3.1. Specifically, the effective policies would ensure relatively short periods to reach the peak of the pandemic. In this sense, the first different is that large a may not be a sign of bad situation. The second difference is that we expect the ratio $R_{t+1,t}$ greater than 1 to indicate more effective policies, since larger $R_{t+1,t}$ implies reaching the peak with a shorter period. Finally, for the ratio $Q_{\tau_t,i1}$ with $i = 2, \ldots, N$, we expect a value greater than 1 to represent a more effective policy compared to the reference individual.

Note that since Africa and America have not reached the peak with obvious reasons by screening the data plots, we do not comment on the values associated with Africa and America much below although the values for these two regions are reported.

3.3.1 Overall Analysis

We first summarize the estimates of a in Table A.4. For both infection and death data, it seems to suggest that in Europe the spread of the virus and the death rate reach the peak slower than the other regions by nature. For Asian & Oceania, the spread of the virus and the death rate tend to reach the peak slightly faster than Europe for both Cases 1 and 2.

We now focus on the values of $R_{t+1,t}$ presented in Figures A.9 and A.10. Consistent with what we find in Section 3.2.1, Europe indeed has more effective polices, as the values of $R_{t+1,t}$ are greater than 1 in the entire period for both Cases 1 and 2. Asia & Oceania have some success, but the situation is not as good as in Europe.

3.3.2 Comparison across Countries

For each region, the reference countries are the same as those in Table A.3. The legend of each sub-plot is ranked by $Q_{\tau_t,i1}$ from largest to smallest at the time period T, however, larger value implies better performance in this case.

For the infection data of Europe, Case 1 of Figure A.11 fully agrees with Case 1 of Figure A.3, i.e., all countries perform better than the reference country. For the death data of Europe, a similar argument applies to Case 2 of Figure A.12 and Case 2 of Figure A.4.

Interestingly, for Asia & Oceania, the downward trending of Cases 1 and 2 in Figures A.3 and A.4 becomes upward trending in Figures A.11 and A.9. Thus, both models confirm that

compared to the reference country, the rest countries in Asia & Oceania have been improving, or the situation of the reference country has been getting out of control.

4   Conclusion

In this paper, we study the trending behaviour of COVID-19 data at country level, and draw attention to some existing econometric tools which are potentially helpful to understand the trend better in the future study. In our empirical study, we find that European countries overall flatten the curves more effectively compared to the other regions, while Asia & Oceania also achieve some success, but the situations are not optimistic as in Europe. Africa and America are still facing serious challenges in terms of managing the spread of the virus, and reducing the death rate, although in Africa the virus spreads slower and has lower death rate than the other regions by nature. By comparing the performances of different countries, our results incidentally agree with Gu et al. (2020), though different approaches and models are considered. For example, both works agree that countries such as USA, UK and Italy perform relatively poorly; on the other hand, Australia, China, Japan, Korea, and Singapore perform relatively better.

References

Bai, J. and Ng, S. (2002), 'Determining the number of factors in approximate factor models', *Econometrica* **70**(1), 191–221.

Bai, J. and Ng, S. (2019), Matrix completion, counterfactuals, and factor analysis of missing data. Working paper available at https://arxiv.org/abs/1910.06677.

Gao, J., Linton, O. and Peng, B. (2020), 'Inference on a semiparametric model with global power law and local nonparametric trends', *Econometric Theory* **36**(2), 223–249.

Gu, J., Yan, H., Huang, Y., Zhu, Y., Sun, H., Zhang, X., Wang, Y., Qiu, Y. and Chen, S. (2020), Better strategies for containing COVID-19 epidemics — A study of 25 countries via an extended varying coefficient seir model. Working paper available at https://doi.org/10.1101/2020.04.27.20081232.

Hong, Y. and Li, H. (2005), 'Nonparametric specification testing for continuous-time models with applications to term structure of interest rates', *The Review of Financial Studies* **18**(1), 37–84.

Li, Q. and Racine, J. (2006), *Nonparametric Econometrics Theory and Practice*, Princeton University Press.

Linton, O. (2020), When will the COVID-19 pandemic peak? Working paper available at http://covid.econ.cam.ac.uk/linton-uk-covid-cases-predicted-peak.

Liu, L., Moon, H. R. and Schorfheide, F. (2020), Panel forecasts of country-level covid-19 infections. https://www.nber.org/papers/w27248.

Phillips, P. C. B. (2007), 'Regression slowly varying regressors and nonlinear trends', *Econometric Theory* **23**(4), 557–614.

Robinson, P. M. (1989), 'Chapter 15: Nonparametric estimation of time-varying parameters', *Statistical Analysis and Forecasting of Economic Structural Change* pp. 253–264.

Robinson, P. M. (1991), 'Chapter 13: Time-varying nonlinear regression', *Economic Structural Change* pp. 179–190.

Robinson, P. M. (2012), 'Inference on power law spatial trends', *Bernoulli* **18**(2), 644–677.

Su, L., Miao, K. and Jin, S. (2019), On factor models with random missing: Em estimation,inference, and cross validation. Working paper available at https://ink.library.smu.edu.sg/soe_research/2231/.

Su, L. and Wang, X. (2017), 'On time-varying factor models: Estimation and testing', *Journal of Econometrics* **198**(1), 84–101.

Appendix A

In what follows, $O(1)$ stands for a constant, and may be different at each appearance. Without loss of generality, let $b_{1T} \leq b_{2T} \leq \cdots \leq b_{NT}$ in what follows.

Lemma A.1

Consider the model stated in (2.1) and (2.2). Under Assumption 1, as $(N,T) \to (\infty, \infty)$,

1. $\sup_{u\in\mathbb{D}} \left\| \frac{1}{NT} \sum_{t=1}^{T} \mathbb{I}_t \frac{G(\tau_t)}{T^a} \frac{G(\tau_t)'}{T^a} \mathbb{I}_t K_h(\tau_t - u) - \frac{1}{N}\mathcal{G}(u)\mathcal{G}(u)' \right\|^2$
$= O\left(\frac{1}{T^{\min\{\nu_1,\nu_2\}}} + \frac{\sharp\mathbb{N}_u^c}{N} + h^\mu \right);$

2. $\sup_{u\in\mathbb{D}} \left| \frac{1}{NT} \sum_{t=1}^{T} G(\tau_t)'\mathbb{I}_t G(\tau_t) \left(\beta^*(\tau_t, b_i^*)\right)^2 K_h(\tau_t - u) - \frac{1}{N}\sum_{i\in\mathbb{N}_u} \beta^*(u, b_i^*)^2 g_i(u)^2 \right|$
$= O\left(\frac{1}{T^{\min\{\nu_1,\nu_2\}}} + \frac{\sharp\mathbb{N}_u^c}{N} + h^\mu \right).$

Proof of Lemma A.1:

(1). Write

$$\sup_{u\in\mathbb{D}} \left\| \frac{1}{NT} \sum_{t=1}^{T} \mathbb{I}_t \frac{G(\tau_t)}{T^a} \frac{G(\tau_t)'}{T^a} \mathbb{I}_t K_h(\tau_t - u) - \frac{1}{N}\mathcal{G}(u)\mathcal{G}(u)' \right\|^2$$

$$= \sup_{u \in \mathbb{D}} \frac{1}{N^2} \sum_{i \in \mathbb{N}_u} \sum_{j \in \mathbb{N}_u} \left\{ \frac{1}{T} \sum_{t=1}^{T} F_i(u) F_j(u) \mathbb{I}(t \geq b_{iT}) \mathbb{I}(t \geq b_{jT}) K_h(\tau_t - u) - F_i(u) F_j(u) \right\}^2$$

$$+ O\left(\frac{1}{T^{\nu_2}} + \frac{\sharp \mathbb{N}_u^c}{N} \right)$$

$$= \sup_{u \in \mathbb{D}} \frac{1}{N^2} \sum_{i \in \mathbb{N}_u} \left\{ \int_{b_i^*}^{1} F_i(u)^2 K_h(w - u) dw - F_i(u)^2 \right\}^2$$

$$+ \sup_{u \in \mathbb{D}} \frac{2}{N^2} \sum_{i \in \mathbb{N}_u} \sum_{j \in \mathbb{N}_u, j < i} \left\{ \int_{b_i^*}^{1} F_i(u) F_j(u) K_h(w - u) dw - F_i(u) F_j(u) \right\}^2$$

$$+ O\left(\frac{1}{T^{\min\{\nu_1, \nu_2\}}} + \frac{\sharp \mathbb{N}_u^c}{N} \right)$$

$$= \sup_{u \in \mathbb{D}} \frac{2}{N^2} \sum_{i \in \mathbb{N}_u} \sum_{j \in \mathbb{N}_u, j < i} \left\{ \int_{b_i^*}^{1} F_i(u) F_j(u) K_h(w - u) dw - F_i(u) F_j(u) \right\}^2$$

$$+ O\left(\frac{1}{T^{\min\{\nu_1, \nu_2\}}} + \frac{\sharp \mathbb{N}_u^c}{N} \right)$$

$$= \sup_{u \in \mathbb{D}} \frac{2}{N^2} \sum_{i \in \mathbb{N}_u} \sum_{j \in \mathbb{N}_u, j < i} \left\{ \int_{-1}^{1} F_i(u + hw) F_j(u + hw) K(w) dw - F_i(u) F_j(u) \right\}^2$$

$$+ O\left(\frac{1}{T^{\min\{\nu_1, \nu_2\}}} + \frac{\sharp \mathbb{N}_u^c}{N} \right)$$

$$= O\left(\frac{1}{T^{\min\{\nu_1, \nu_2\}}} + \frac{\sharp \mathbb{N}_u^c}{N} + h^\mu \right),$$

where the first equality follows from the second condition of (2.2) and the construction of $\mathbb{C}$; the second equality follows from the definition of Riemann integral and the first condition of (2.2); the third equality follows from by focusing on the leading term only; the fourth equality follows by the construction of $\mathbb{C}$ and integration by substitution; and the fifth equality follows from Assumption 1.2.

(2). Similar to the first result, the second result follows. The proof is complete now. ∎

Proof of Theorem 2.1:

(1). We expand (2.7) as follows.

$$\frac{\lambda_u}{T^{2a}} \ell_u = \frac{1}{T^{2a}} \Sigma(u) \ell_u = \frac{1}{NT^{2a+1}} \sum_{t=1}^{T} \mathbb{I}_t G(\tau_t) G(\tau_t)' \mathbb{I}_t K_h(\tau_t - u) \ell_u$$

$$+ \frac{1}{NT^{2a+1}} \sum_{t=1}^{T} \mathbb{I}_t \mathcal{E}_t \mathcal{E}_t' \mathbb{I}_t K_h(\tau_t - u) \ell_u$$

$$+ \frac{1}{NT^{2a+1}} \sum_{t=1}^{T} \mathbb{I}_t G(\tau_t) \mathcal{E}_t' \mathbb{I}_t K_h(\tau_t - u) \ell_u$$

$$+ \frac{1}{NT^{2a+1}} \sum_{t=1}^{T} \mathbb{I}_t \mathcal{E}_t G(\tau_t)' \mathbb{I}_t K_h(\tau_t - u) \ell_u$$

$$:= A_1 + \cdots + A_4. \tag{A.1}$$

14

Below, we investigate A_1 to A_4 one by one.

$$\sup_{u \in \mathbb{D}} \|A_2\| = \sup_{u \in \mathbb{D}} \left\| \frac{1}{NT^{2a+1}} \sum_{t=1}^{T} \mathbb{I}_t \mathcal{E}_t \mathcal{E}_t' \mathbb{I}_t K_h(\tau_t - u) \ell_u \right\|$$

$$\leq \frac{1}{T^{2a}} \sup_{u \in \mathbb{D}} \left\{ \frac{1}{NT} \sum_{t=1}^{T} \mathcal{E}_t' \mathbb{I}_t \mathcal{E}_t K_h(\tau_t - u) \right\}^{1/2} \left\{ \frac{1}{NT} \sum_{t=1}^{T} \mathcal{E}_t' \mathbb{I}_t \mathcal{E}_t K_h(\tau_t - u) \right\}^{1/2}$$

$$= O_P(1) \frac{1}{T^{2a}} \cdot \delta_T^{1/2} \cdot \delta_T^{1/2} = O_P\left(\frac{\delta_T}{T^{2a}} \right),$$

where the first inequality follows from Cauchy-Schwarz inequality; the second equality follows from Lemma A.1 and Assumption 1.3

For A_3, write

$$\sup_{u \in \mathbb{D}} \|A_3\| = \sup_{u \in \mathbb{D}} \left\| \frac{1}{NT^{2a+1}} \sum_{t=1}^{T} \mathbb{I}_t G(\tau_t) \mathcal{E}_t' \mathbb{I}_t K_h(\tau_t - u) \ell_u \right\|$$

$$\leq \frac{1}{T^a} \sup_{u \in \mathbb{D}} \left\{ \frac{1}{NT} \sum_{t=1}^{T} \frac{G(\tau_t)'}{T^a} \mathbb{I}_t \frac{G(\tau_t)}{T^a} K_h(\tau_t - u) \right\}^{1/2} \left\{ \frac{1}{NT} \sum_{t=1}^{T} \mathcal{E}_t' \mathbb{I}_t \mathcal{E}_t K_h(\tau_t - u) \right\}^{1/2}$$

$$= O_P(1) \frac{1}{T^a} \cdot 1 \cdot \delta_T^{1/2} = O_P\left(\frac{\delta_T^{1/2}}{T^a} \right),$$

where the first inequality follows from Cauchy-Schwarz inequality; the second equality follows from Lemma A.1 and Assumption 1.3. Similarly,

$$\sup_{u \in \mathbb{D}} \|A_4\| = O_P\left(\frac{\delta_T^{1/2}}{T^a} \right).$$

Thus, we obtain that

$$\sup_{u \in \mathbb{D}} \left\| \frac{\lambda_u}{T^{2a}} \ell_u - A_1 \right\| = \sup_{u \in \mathbb{D}} \left\| \frac{\lambda_u}{T^{2a}} \ell_u - \frac{1}{N} \mathcal{G}(u) \mathcal{G}(u)' \ell_u + \frac{1}{N} \mathcal{G}(u) \mathcal{G}(u)' \ell_u - A_1 \right\|$$

$$\leq \sum_{j=2}^{4} \sup_{u \in \mathbb{D}} \|A_j\| = O_P\left(\frac{\delta_T^{1/2}}{T^a} \right),$$

which, in connection with Lemma A.1, yields that

$$\sup_{u \in \mathbb{D}} \left\| \frac{\lambda_u}{T^{2a}} \ell_u - \frac{1}{N} \mathcal{G}(u) \mathcal{G}(u)' \ell_u \right\| = O_P(\phi_{1,NT}), \tag{A.2}$$

where $\phi_{1,NT} = \frac{\delta_T^{1/2}}{T^a} + \left\{ \frac{1}{T^{\min\{\nu_1, \nu_2\}}} + \frac{\sharp \mathbb{N}_u^c}{N} + h^\mu \right\}^{1/2}$. Thus, the first argument $\sup_{u \in \mathbb{D}} \|\ell_u \ell_u' - P_{\mathcal{G}(u)}\| = O_P(\phi_{1,NT})$ follows.

Left multiplying (A.2) by $\frac{\mathcal{G}(u)'}{\sqrt{N}}$, we can write

$$\sup_{u \in \mathbb{D}} \left| \frac{\lambda_u}{T^{2a}} \frac{\mathcal{G}(u)' \ell_u}{\sqrt{N}} - \frac{\mathcal{G}(u)' \mathcal{G}(u)}{N} \cdot \frac{\mathcal{G}(u)' \ell_u}{\sqrt{N}} \right| = O_P(\phi_{1,NT}),$$

15

which further leads to

$$\sup_{u \in \mathbb{D}} \left| \frac{\lambda_u}{T^{2a}} - \frac{\mathcal{G}(u)'\mathcal{G}(u)}{N} \right| = O_P(\phi_{1,NT}). \tag{A.3}$$

Thus, the proof of the first result is complete.

(2). Write

$$
\begin{aligned}
\frac{1}{\sharp\mathbb{C}} \sum_{t \in \mathbb{C}} \frac{\lambda_{\tau_t}}{T^{2a}} &= \frac{1}{\sharp\mathbb{C}} \sum_{t \in \mathbb{C}} \left(\frac{\lambda_{\tau_t}}{T^{2a}} - \frac{\mathcal{G}(\tau_t)'\mathcal{G}(\tau_t)}{N} \right) + \frac{1}{\sharp\mathbb{C}} \sum_{t \in \mathbb{C}} \frac{\mathcal{G}(\tau_t)'\mathcal{G}(\tau_t)}{N} \\
&= \frac{1}{\sharp\mathbb{C}} \sum_{t \in \mathbb{C}} \frac{\mathcal{G}(\tau_t)'\mathcal{G}(\tau_t)}{N} + O_P(\phi_{1,NT}) \\
&= \int_{\mathbb{D}} \bar{g}(u)^2 du + O_P(\phi_{1,NT} + \phi_{2,N}) = 1 + O_P(\phi_{1,NT} + \phi_{2,N}),
\end{aligned}
$$

where the second equality follows from (A.3) and the construction of $\mathbb{C}$; and the third equality follows from Assumption 1.2. Then

$$\ln \left\{ \frac{1}{\sharp\mathbb{C}} \sum_{t \in \mathbb{C}} \lambda_{\tau_t} \right\} - 2a \ln T = O_P(\phi_{1,NT} + \phi_{2,N}),$$

which gives that $\hat{a} - a = O_P(\frac{\phi_{1,NT} + \phi_{2,N}}{\ln T})$. Thus, the second result follows.

(3)-(4). By the first result, the third and fourth results follow immediately. The proof is complete.
∎

16

Table A.1: Available Sample

	Infection		Death	
	N	T	N	T
AF	48	62	23	50
AM	43	98	20	61
AO	48	123	25	108
EU	49	98	41	69

Table A.2: Estimate of a for Model (2.1)

		Case 1			Case 2		
		$\widehat{h}$	h_L	h_R	$\widehat{h}$	h_L	h_R
Infection	AF	0.239	0.240	0.239	0.393	0.393	0.393
	AM	0.274	0.277	0.272	0.402	0.402	0.402
	AO	0.262	0.263	0.262	0.409	0.401	0.405
	EU	0.328	0.329	0.327	0.449	0.449	0.448
Death	AF	0.021	0.022	0.020	0.321	0.322	0.321
	AM	0.285	0.286	0.285	0.445	0.445	0.445
	AO	0.133	0.133	0.132	0.367	0.366	0.365
	EU	0.235	0.235	0.234	0.409	0.401	0.405

Table A.3: Reference Countries for Figures A.3, A.4, A.11, A.12

	Infection	Death
AF	South Africa	Egypt
AM	Brazil	Brazil
AO	India	India
EU	Russia	United Kingdom

Table A.4: Estimate of a for Model (2.9)

		Case 1			Case 2		
		$\widehat{h}$	h_L	h_R	$\widehat{h}$	h_L	h_R
Infection	AF	0.229	0.230	0.229	0.396	0.396	0.396
	AM	0.187	0.188	0.186	0.358	0.358	0.357
	AO	0.210	0.212	0.209	0.393	0.394	0.392
	EU	0.164	0.164	0.164	0.375	0.375	0.375
Death	AF	0.108	0.109	0.107	0.339	0.339	0.339
	AM	0.096	0.096	0.095	0.367	0.367	0.367
	AO	0.144	0.146	0.143	0.373	0.373	0.372
	EU	0.103	0.104	0.102	0.345	0.345	0.344

Figure A.1: Model 1 — $R_{t+1,t}$ of Infection Data. The left and right panels are Case 1 and Case 2 respectively.
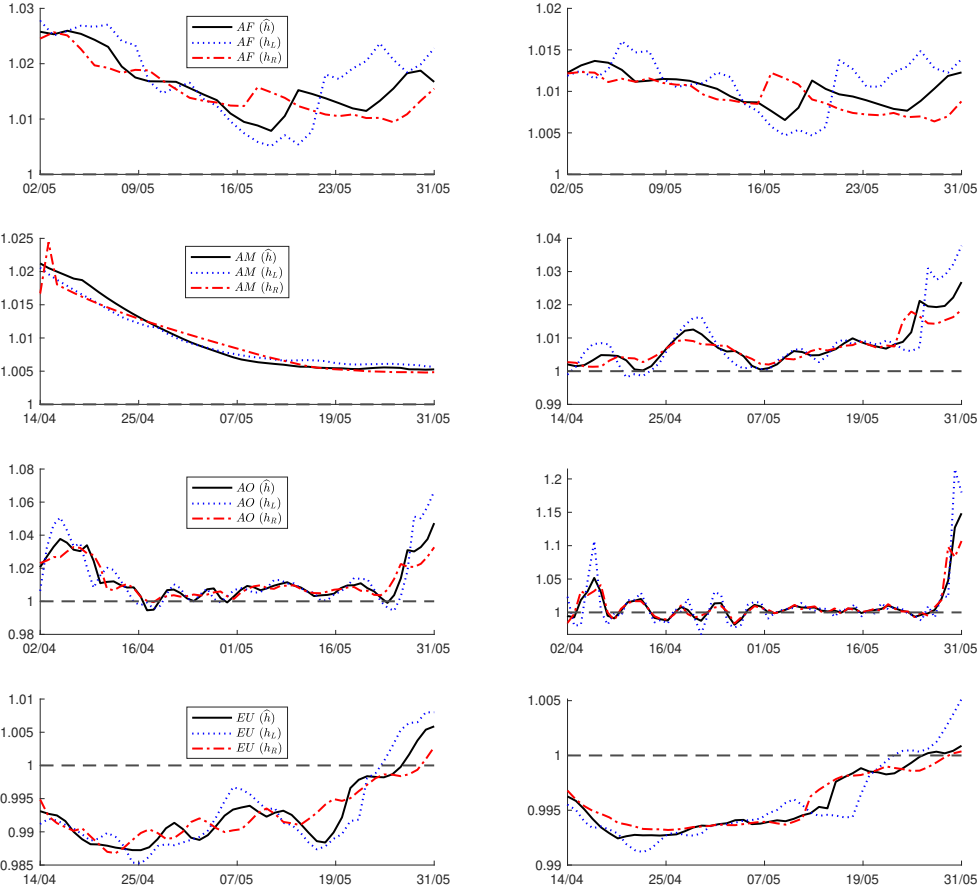
Figure A.2: Model 1 — $R_{t+1,t}$ of Death Data. The left and right panels are Case 1 and Case 2 respectively.
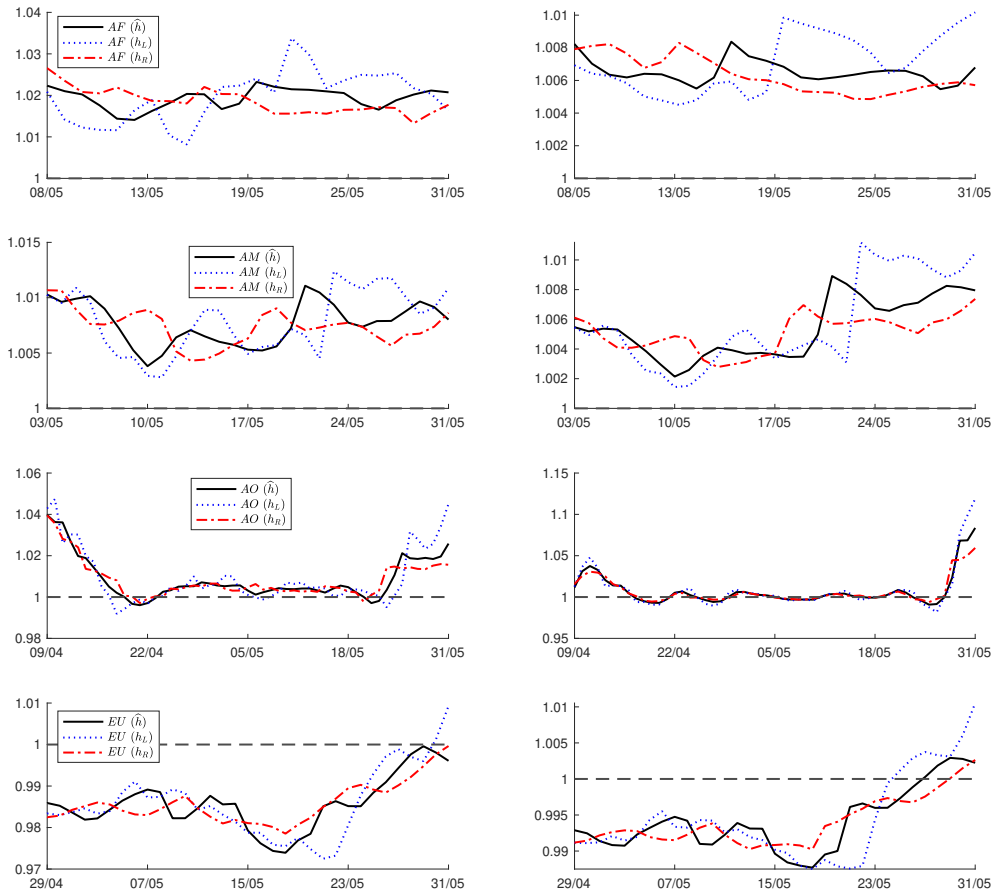
Figure A.3: Model 1 — $Q_{\tau_t,i1}$ of Infection Data. The top and bottom panels are Case 1 and Case 2 respectively. The reference countries are presented in Table A.3.
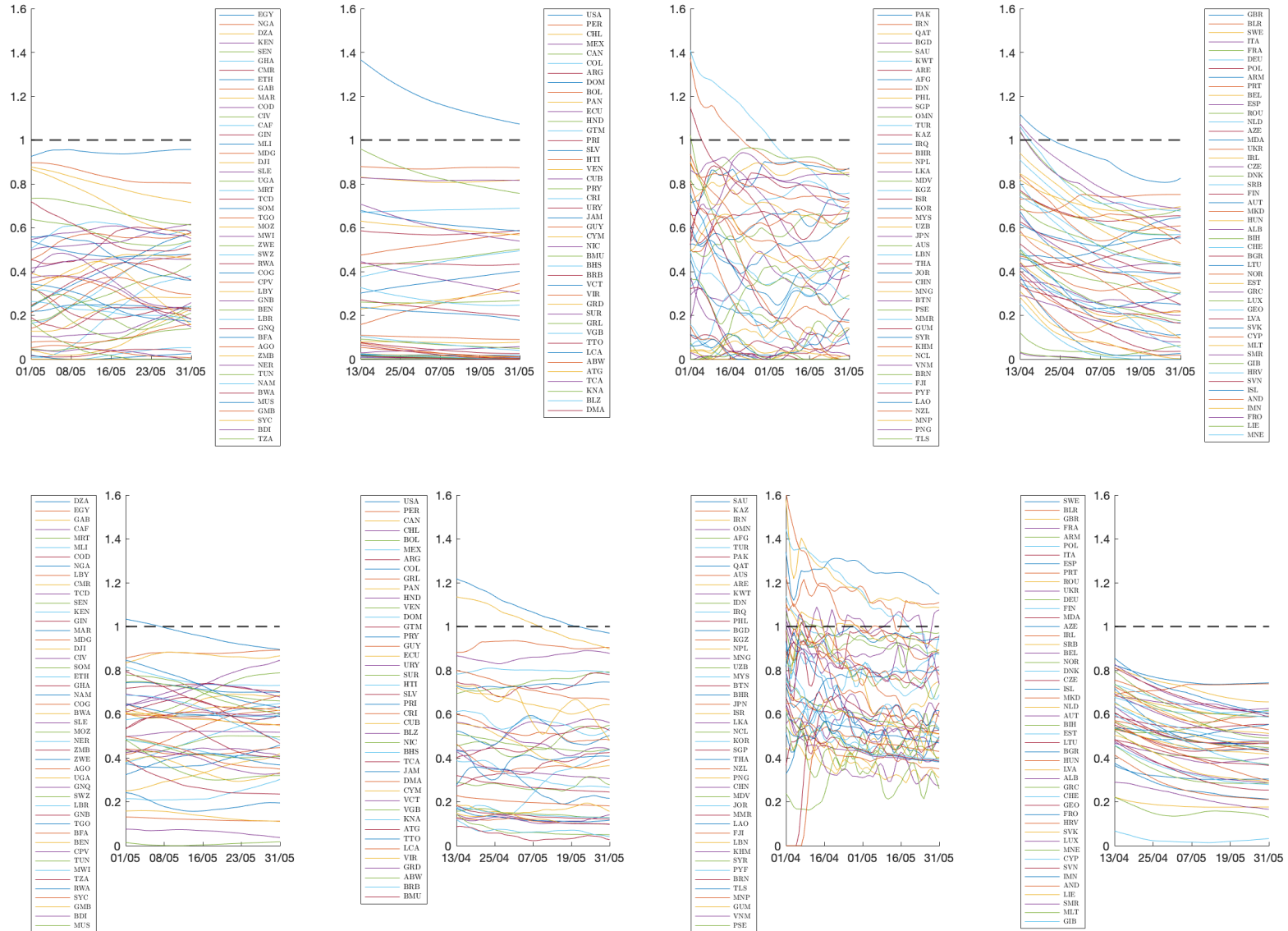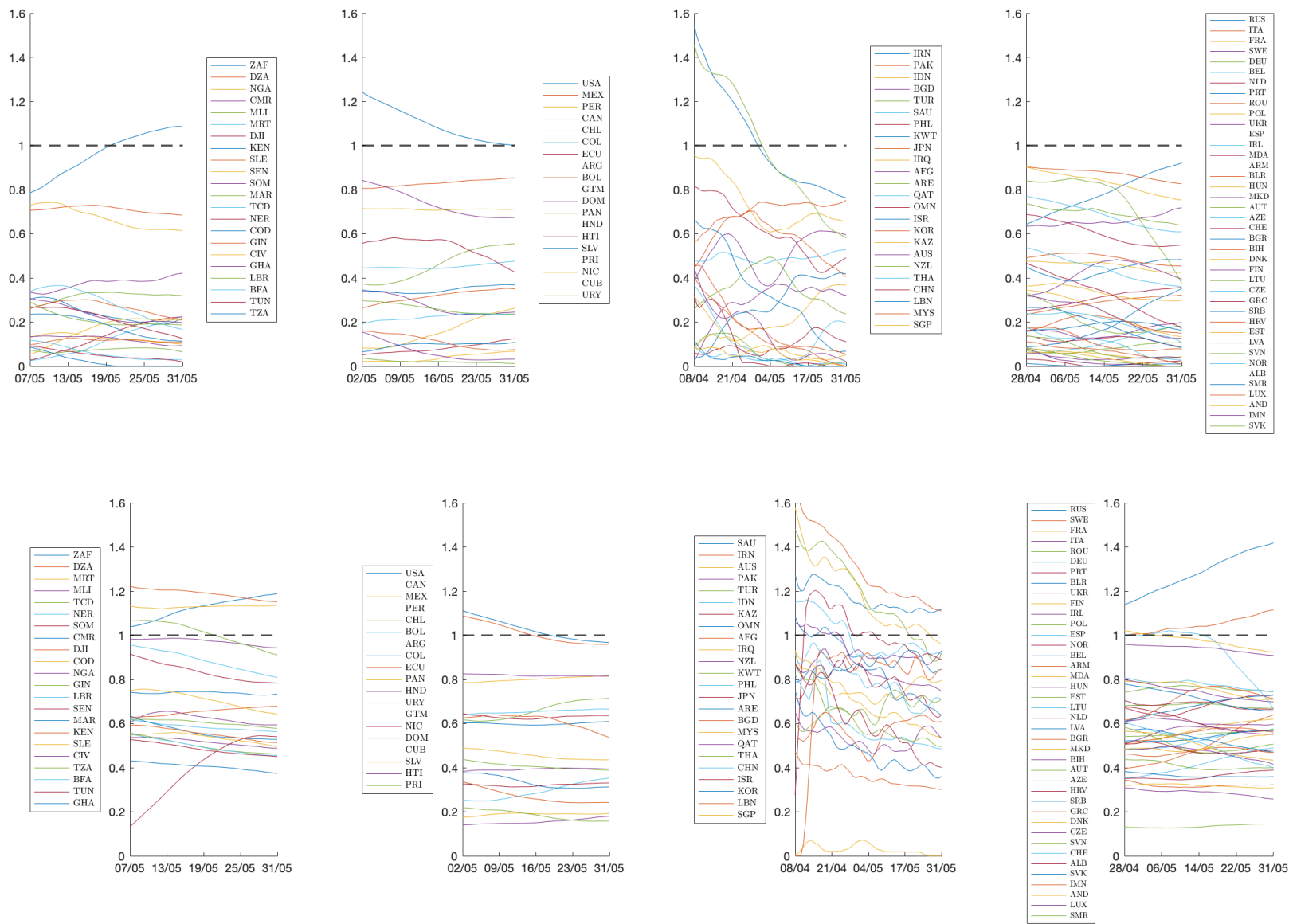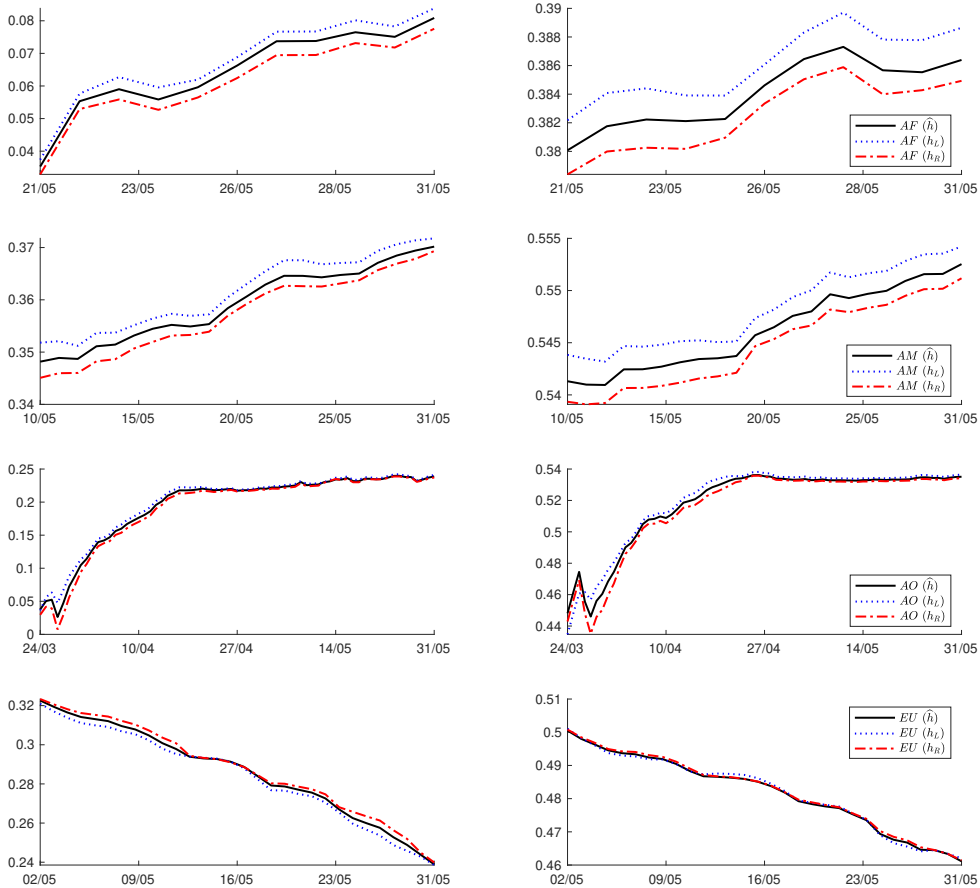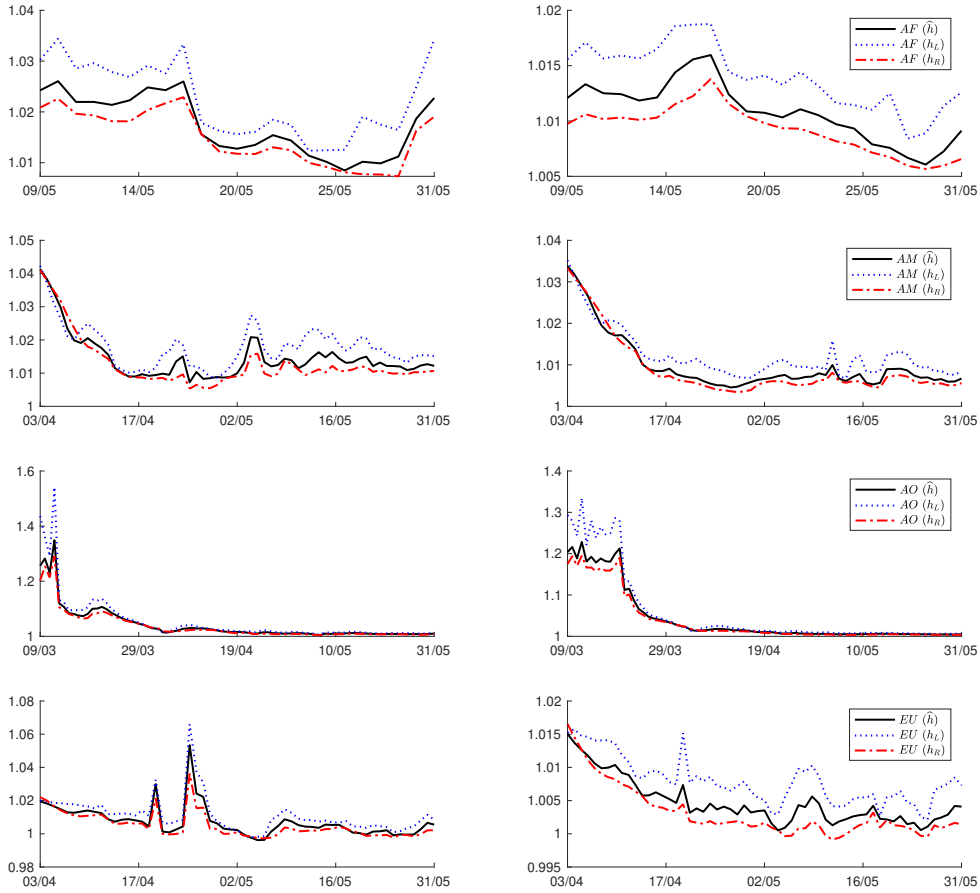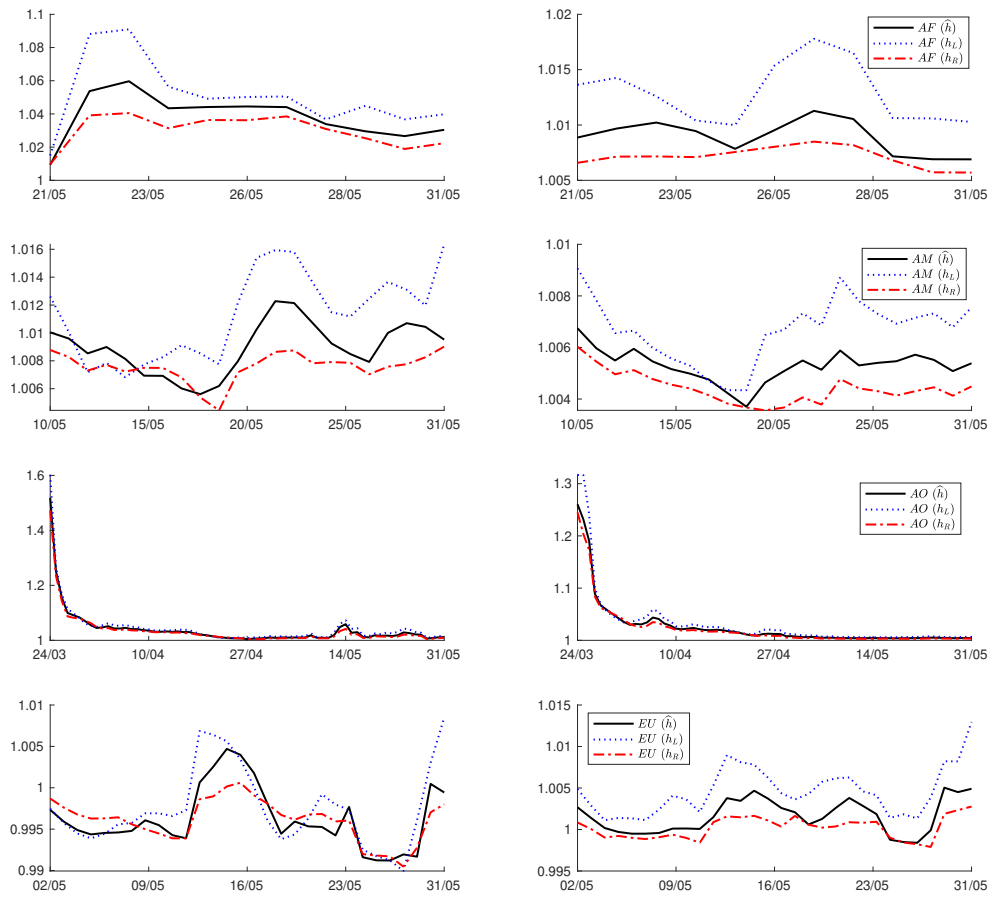
Figure A.4: Model 1 — $Q_{\tau_t, i1}$ of Death Data. The top and bottom panels are Case 1 and Case 2 respectively. The reference countries are presented in Table A.3.

Figure A.5: Model 1 — Estimated a of Infection Data using Rolling Window. The left and right panels are Case 1 and Case 2 respectively.
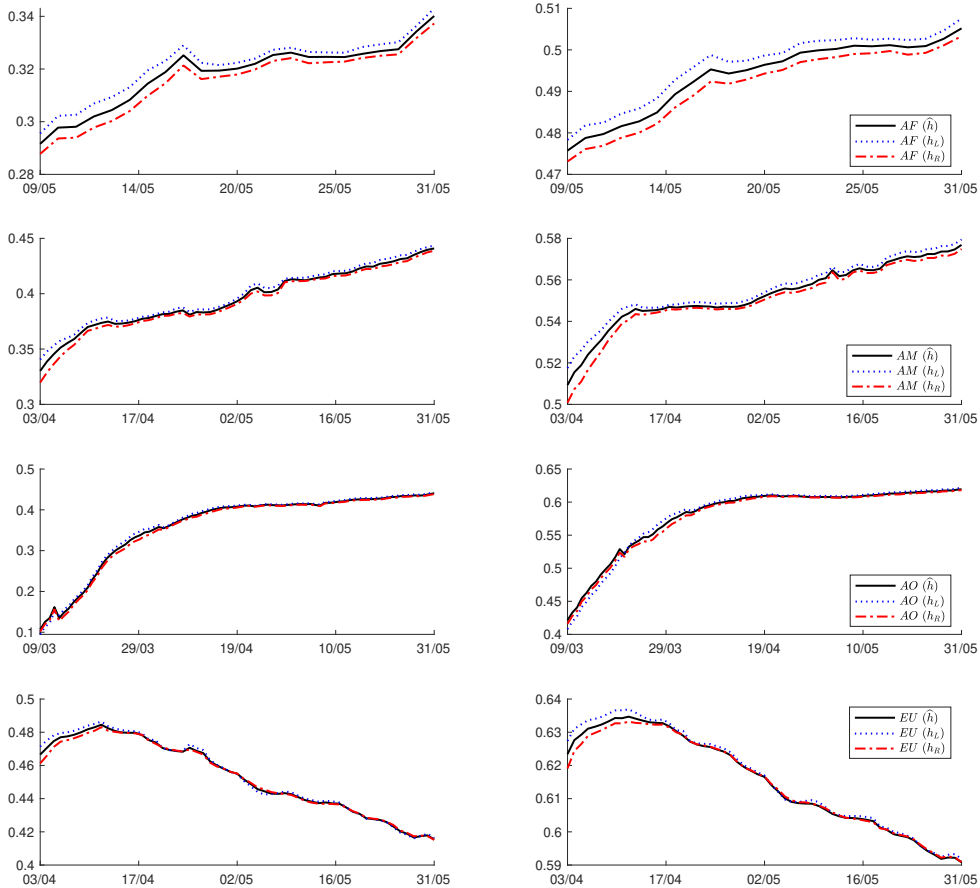
Figure A.6: Model 1 — Estimated a of Death Data using Rolling Window. The left and right panels are Case 1 and Case 2 respectively.

Figure A.7: Model 1 — $\bar{R}$ of Infection Data using Rolling Window. The left and right panels are Case 1 and Case 2 respectively.

Figure A.8: Model 1 — $\bar{R}$ of Death Data using Rolling Window. The left and right panels are Case 1 and Case 2 respectively.

Figure A.9: Model 2 — $R_{t+1,t}$ of Infection Data. The left and right panels are Case 1 and Case 2 respectively.
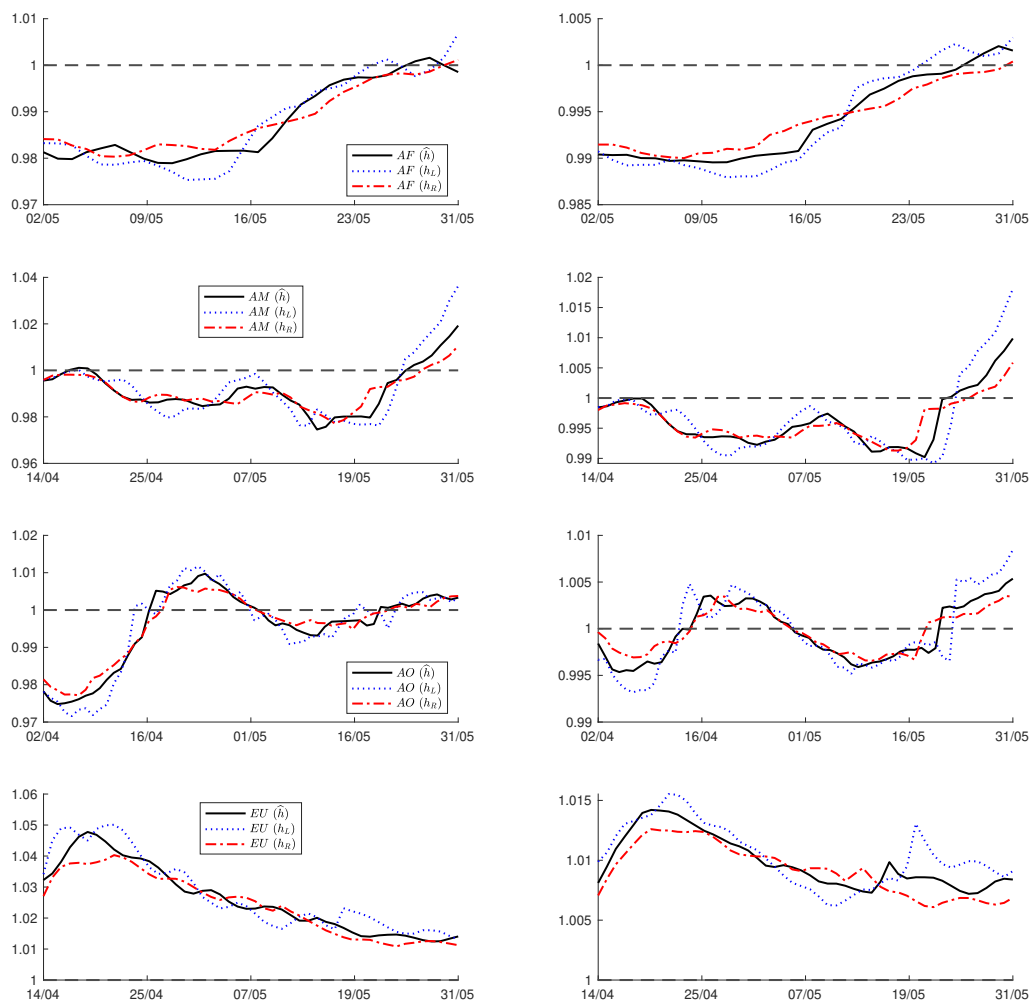
Figure A.10: Model 2 — $R_{t+1,t}$ of Death Data. The left and right panels are Case 1 and Case 2 respectively.
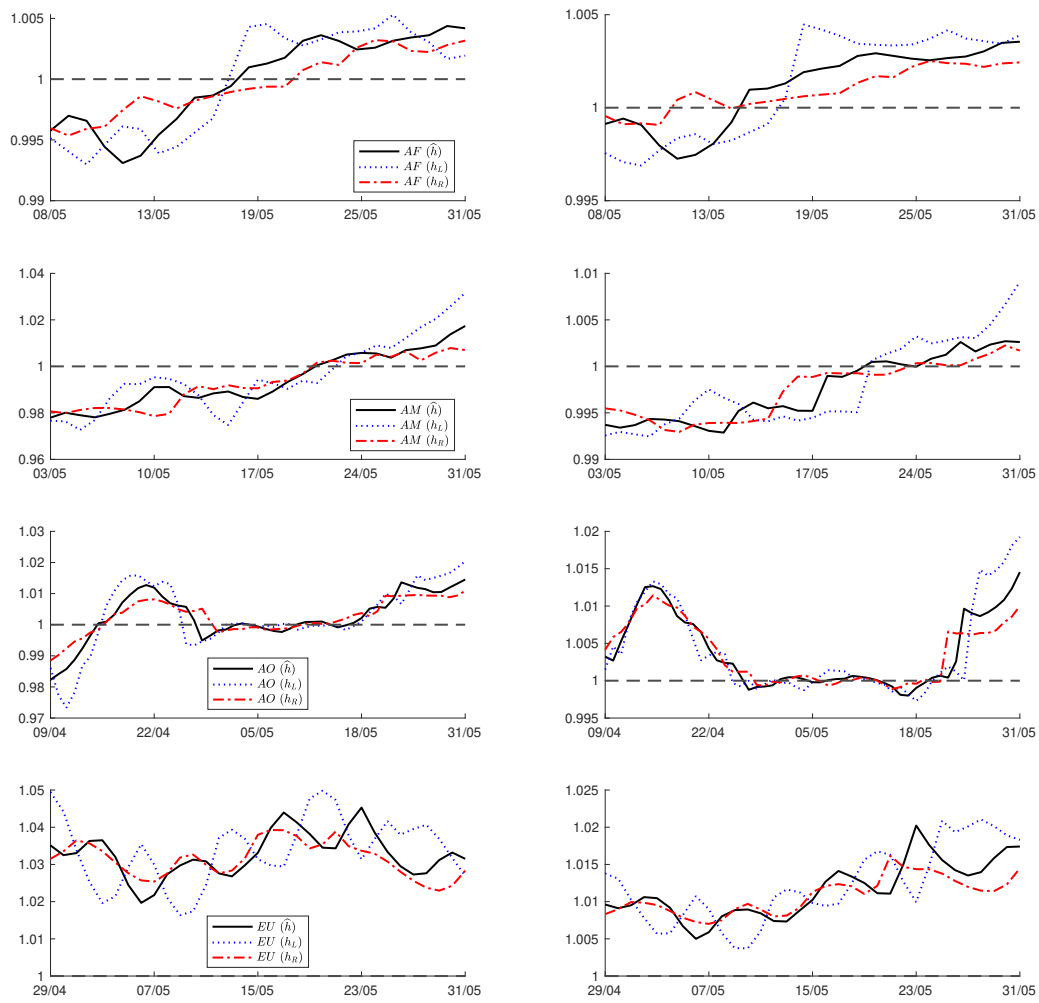
Figure A.11: Model 2 — $Q_{\tau_t, i1}$ of Infection Data. The top and bottom panels are Case 1 and Case 2 respectively. The reference countries are presented in Table A.3.
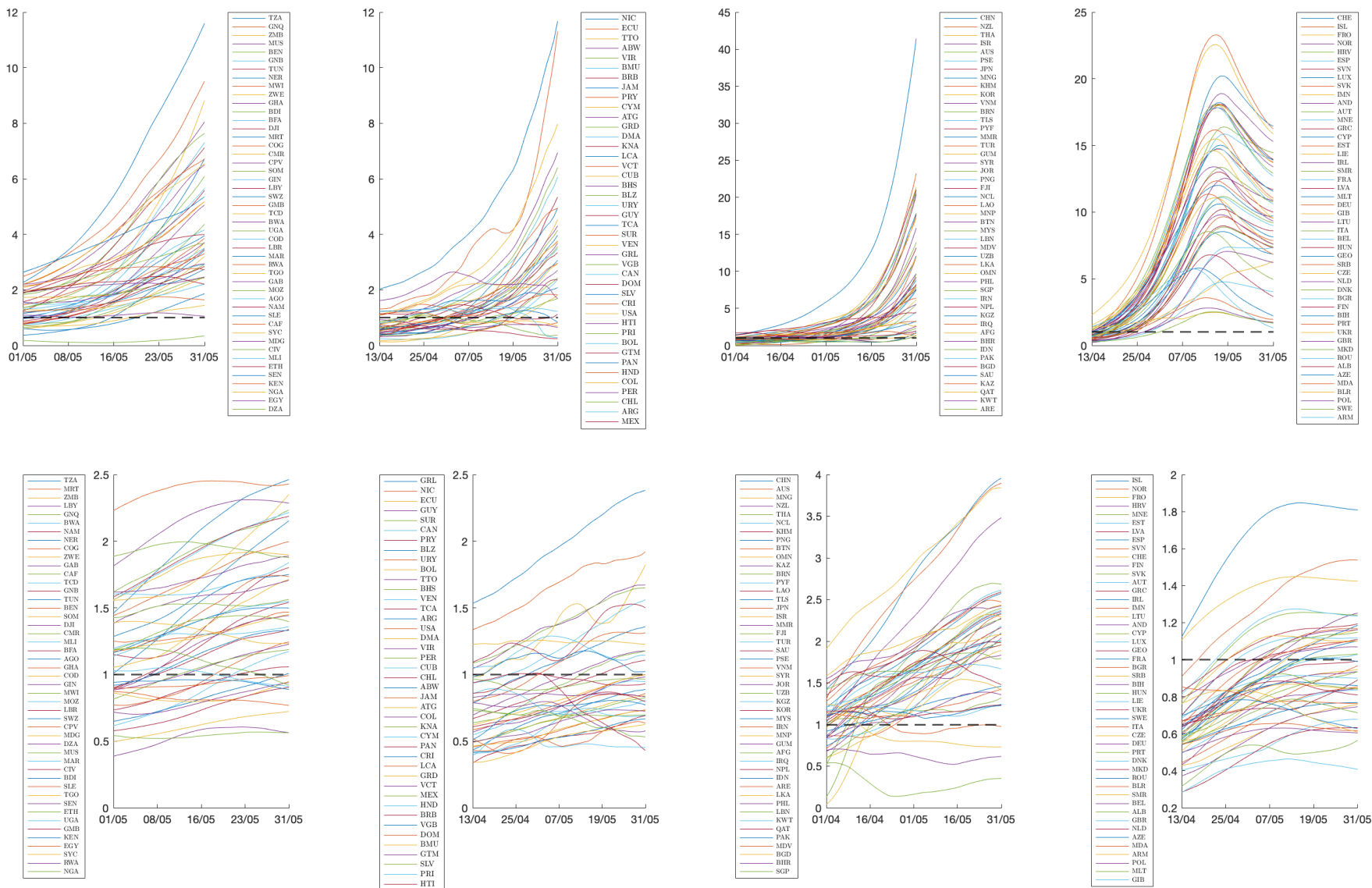
Figure A.12: Model 2 — $Q_{\tau_t,i1}$ of Death Data. The top and bottom panels are Case 1 and Case 2 respectively. The reference countries are presented in Table A.3.